Proceedings of the ASME 2019
Dynamic Systems and Control Conference
DSCC2019
October 8-11, 2019, Park City, UT, USA

DSCC2019-9153

ANALYSIS OF REFERENCE SHAPING CONTROL FOR IMPROVED YAW STABILITY IN A STEER-BY-WIRE VEHICLE

Srivatsan Srinivasan, Matthias J. Schmid*, Venkat N. Krovi
Department of Automotive Engineering
Clemson University International Center for Automotive Research
Greenville, South Carolina 29607, USA
srivats@g.clemson.edu, schmidm@clemson.edu, vkrovi@clemson.edu

ABSTRACT

Incorporation of electronic yaw stabilization in on-road vehicles can take many forms. Although the most popular ones are differential braking and torque distribution, a potentially better alternative would be the inclusion of a controller into the steering process. However, this is not often pursued in mechanically-coupled steering systems since the controller could work against the driver's intentions creating potential challenges to safety. The growing adoption of steer-by-wire (SbW) systems now in autonomous/semi-autonomous vehicles offers an opportunity to simplify the incorporation of such steering-controller based assistance. Most current steering-assistance systems focus either on adaptive steering control (adaptive power steering and gear ratios) or on total steering control in autopilot functions (lane keeping control). Such steering-controllers (incorporated via SbW modality) can improve driving performance and maneuverability and contribute to the overall suite of active-safety vehicle systems. In this study, we introduce a new pure-feedforward (open loop) controller for the steer-by-wire system based on the concept of reference shaping control aimed at reducing the vibration/oscillation caused in vehicles during fast (evasive) maneuvers.

Keywords: steer-by-wire, steering control, yaw stability, input shaping, driver-assistance

INTRODUCTION

Vehicle yaw and rollover stability during safety-critical maneuvers while the driver is out of the loop has been a topic of interest for quite some time owing to recent advancements in advanced driver assistance systems (ADAS), semi-autonomous vehicles and autonomous vehicles. Since 2014, ESC of some form has been mandatory in all new cars in the USA as several studies concluded that a third of all fatal accidents can be prevented using this technology [1-2]. Traditionally, vehicle yaw stabilization has been realized utilizing either differential braking or torque distribution whereas steering control has been employed only for assistive systems such as Lane Keep Systems (LKS).

In modern vehicles, steering control is an essential component for several of the active safety systems such as Lane Keep, Emergency Braking, Active Rollover Safety, Electronic Stability Control, etc. In a mechanical steering system, variable time delays exist between the driver's inputs and the response of the vehicle dynamic states during a critical steering maneuver. On the other hand, a sideslip or rollover may occur even in a vehicle with a traditional stability control system due to non-uniform delays in active brake actuators. This is one of the main reasons why drive-by-wire is a key enabler for autonomous vehicle development. Here, safety can be improved by employing computer-mediated intervention of vehicle controls as the direct steering wheel input can be simply bypassed/modified [3]. Additionally, the fast response time and increased accuracy contributes to improved maneuverability requiring only small maneuvering angles. In our work, we explore the possibility of extending steering control as a means for yaw stabilization by introducing a feedforward steer-by-wire controller based on the concept of reference shaping.

By-wire has been the prevailing norm in certain aviation application for decades and a growing trend in SbW vehicles can be observed recently. With their Q50, Infiniti became the first brand to incorporate SbW systems (called direct adaptive steering technology) into their vehicles in 2014., hence, this has opened an entirely new aspect in ADAS for potential development. Although initially faced with negative reviews, the

*Corresponding Author

improved version released in 2017 has been widely appreciated [4]. A recent "research and markets" survey reported several or the leading OEMs rapidly progressing towards deployment of preliminary forms of SbW vehicles [5]. This allows for new opportunities in steering controller development for vehicle safety systems with a variety of open-ended research areas [6]. Here, we focus on developing a new steering controller that is effective for ADAS as well as semi-autonomous and/or autonomous vehicles.

STEERING CONTROL FOR YAW STABILITY

The main objective of a (supportive) steering controller is to compensate for the potential shortcomings in a reference input, arising from either a human driver or from an algorithm in the form of a planner. Typically, the driver must perform two main tasks when operating a vehicle: (i) following a determined path and (ii) disturbance attenuation (yaw control). While usually being able to perform the second task well in regular driving situations, drivers might be overwhelmed by the simultaneous execution of both tasks in emergency / highly dynamic situations when met with unusual disturbances. The response might get delayed, causing stability issues. Yaw stability systems (ESC, VDC, etc.) gained popularity for aiding a driver in the task of disturbance attenuation such that the focus can be entirely on path following. In driving situations/maneuvers that are manageable, the driver compensates for instabilities caused by a disturbance (such as obstacle avoidance) by rather using the steering wheel input than applying brakes. An SbW vehicle simplifies this as the steering wheel is merely an input device whose reference can be ***modulated*** by a computer.

Recent Literature

A controller based on the μ control strategy was proposed in [7] for a four-wheel steer-by-wire vehicle (FSV). Recently, a few more complex closed-loop control algorithms were produced by researchers. In [8], a receding horizon yaw moment control is applied to optimally control both the sideslip angle and the yaw rate of the vehicle. Here, the control strategy is guaranteed to be achieved in a finite time. A bi-layer control strategy is proposed in [9] wherein an adaptive sliding mode controller in the upper layer determining the steering angle correction is combined with a terminal sliding mode compensator in the lower layer that employs a neural network-based function to learn the uncertainty bound. The lower layer enforces the commanded angle in a finite time. While beneficial from a control standpoint, this method is complex in development as well as in deployment. A simpler yet robust feedforward-feedback control scheme is proposed in [10] for articulated frame vehicles equipped with a type of electro-hydraulic actuated SbW technology. Not only is the feedforward gain applied to the driver's steering wheel input a tuned parameter, but the proportional gain in the feedback term (with yaw error as an input) needs also to be dialed in. The tuning process of such a controller is often a tedious task and takes multiple levels of testing to calibrate it to perfection.

Remaining Challenges

As the actuation responsibilities in driving move further and further away from the driver, the complexities of the employed algorithms increase multifold. These complexities necessitate a high amount of computation capability to execute successfully in real-time, thus remaining an important factor in their development. Additionally, sensor failures in autonomous vehicles could result in disastrous consequences raising the requirement for techniques such as feedforward control in order to ensure safety even in such scenarios.

This study presents a novel method to track the desired yaw rate in a vehicle during various maneuvers utilizing a feedforward controller applied to steering input. The feedforward function is a finite impulse response filter (FIR) that modifies the reference commands in such a way that 'harmful' components (resulting in excessive dynamic responses) are reduced or removed. Such a strategy is called the reference shaping control, a technique in which the input to the system is shaped to attenuate residual vibration. These algorithm have been explored before in particular relation to crane systems [11][12], but direct deployment to steering control in vehicles has been omitted so far. The vehicle yaw stability controlled by a steering input is often susceptible to residual oscillations during safety critical maneuvers (high speed lane change, evasive maneuvers, etc.) due to system inertia.

Precise position control and rapid (low maneuver time) rest-to-rest motion is critical in these situations. Timely steering-control commands can be layered on the base-steering command to attenuate/compensate unwanted excitations otherwise resulting from the human/planner-generated command signal. In this work, this is implemented via timed impulses that convolve with the driver input to control the vehicle.

In order to evaluate our controller's performance, we refer to a well-established low computational steer-by-wire (SbW) feedback control algorithm detailed in a later section. The equations of motion utilized for developing the controller and plant model are also described in considerable detail. All simulations were performed using MATLAB/SIMULINK [13].

VEHICLE DYNAMICS MODELS

Model Description

The vehicle dynamics models used in this study combine a chassis and a tire-force (Pacejka) model [14] with two distinct versions employed for the chassis dynamics.

Four-wheel vehicle model: This is a planar 4-wheel vehicle model with yaw, roll, and pitch dynamics along with longitudinal and lateral load transfer. This complex 6-DoF model is used as the plant generating 'truth' values for controller validation.

Non-linear bicycle model: This model lumps the left and right wheel on each axle from previous model together. Furthermore, roll and pitch dynamics are neglected leaving only yaw. Thus, the model has two translational and one rotational degree of

freedom. This formulation is the basis for the controller development.

Wheel and tire model: The separate consideration of the wheel contributes an additional degree of freedom in the form of (angular) wheel speeds. Here, the respective driving and braking torques serve as the inputs to each wheel. Additionally, slip angles and slip ratios for individual wheels are modeled. The tire models as the essential element in external force transmission utilize Pacejka's Magic Formula. The model equations utilized in this work are described in the Appendix along with a comprehensive overview of the employed nomenclature. For further details with respect to the models please consult the given references.

Model Validation

We have chosen the standard Fishhook (FH) test as the validation maneuver for our development. As the Fishhook maneuver is a rollover test, it provides a clear distinction between the two employed models with the bicycle model ignoring the roll dynamics entirely. In the Fishhook test, the vehicle is initially driven in a straight line at 50 miles per hour. At time zero, the steering wheel position is linearly increased from 0 to 270 degrees at a rate of 13.5 degrees per second. This position is then hold for two seconds after which the maneuver concludes [15]. Figure 1 depicts the resulting steering wheel profile.

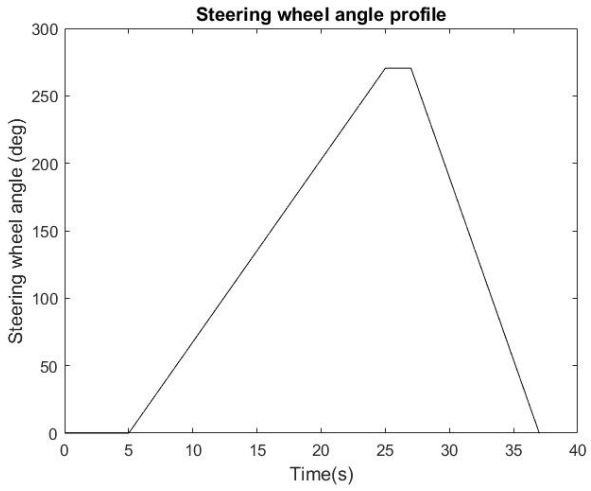

Figure 1: Input steering wheel angle for the FH test

Figure 2 illustrates the emerging vehicle trajectories for both utilized models. While the bicycle model is able to complete the maneuver at 50 mph due to the lack of roll dynamics, the four-wheel model fails given our employed vehicle parameter as it faces a rollover. Figure 3 depicts a successful completion of the maneuver by the four-wheel model when the maneuver speed is decreased to 25 mph.

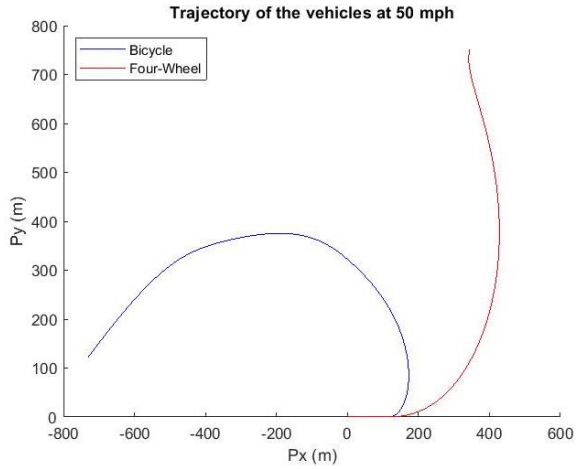

Figure 2: The two models' trajectory at 50 mph. Px and Py are the longitudinal and lateral displacements of the vehicle.

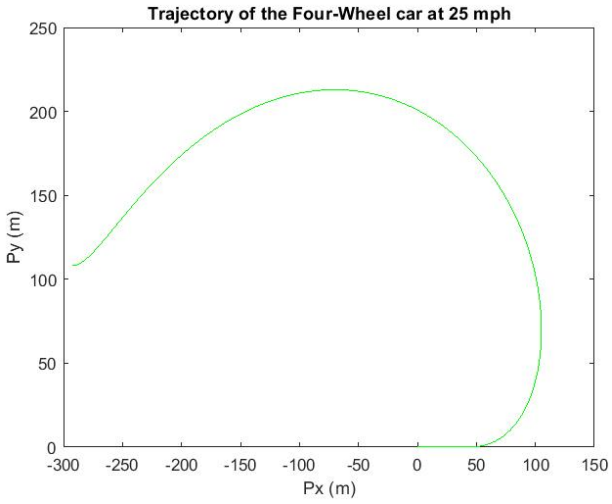

Figure 3: Four-Wheel model completing the maneuver at 25 mph

STEER-BY-WIRE FEEDBACK CONTROLLER

For comparison, we design a standard feedback steering control for yaw stability as detailed in [16]. The effective steering angle applied to the front wheels consists of the sum of the reference driver input (or planner input) and the controller generated compensation to enforce stability and safe maneuvering. The feedback term should only provide stability and safety and must not interfere with the vehicle's desired path as set by the driver. According to [16], the SbW controller's compensation steering angle rate is given by the control law

$$\dot{\delta}_{sbw} = -\dot{\psi} + g(\dot{\psi}) + F(\delta_{driver}) \quad (1)$$

$\dot{\psi}$ is the vehicle's actual yaw rate at the current time and

$$g(\dot{\psi}) = \frac{\cos(\theta_{vf})}{V_x}\left[(l_f - l_p)\ddot{\psi}\cos(\theta_{vf}) + (l_f\dot{\psi}^2 - a_x)\sin(\theta_{vf})\right] \quad (2)$$

Here, θ_{vf} is the vehicle velocity vector's angle at the front tires (with respect to the body-frame), i.e.

$$\dot{\theta}_{vf} = -\dot{\psi} + \left(\frac{cos^2\theta_{vf}}{V_x}\right)a_{yP} + g(\dot{\psi}) \quad (3)$$

with a_{yP} being the lateral acceleration at any point P in the vehicle given by

$$a_{yP} = \frac{L}{ml_r}F_{yf} \quad (4)$$

Lastly, $F(\delta_{driver})$ is a function serving as tuning factor by relating the driver input, δ_{driver}, to the corresponding desired yaw rate, thereby allowing for the selection of under/over-steer behavior. Essentially, this yields the control law utilizing the error in the desired yaw rate $(F(\delta_{driver}) - \dot{\psi})$ as the basis for the feedback compensation term $\dot{\delta}_{sbw}$.

For this study, we have chosen the tuning function $F(\delta_{driver})$ to reflect the desired yaw rate of a neutral steer vehicle as it provides the least distraction to the driver. In addition, it is a suitable condition for superordinate controllers in semi- or full-autonomous vehicles and corresponds to the target performance of current ADAS. Hence, the desired yaw rate given the road curvature R yields $\dot{\psi}_{des} = \frac{V_x}{R}$. With the relation between δ_{driver} and R given by $\frac{1}{R} = \frac{\delta_{driver}}{l_f + l_r}$ and with K_{sbw} being a feedback gain to fine tune the controller performance (ideal value 1), the tuning function becomes

$$F(\delta_{driver}) = \frac{K_{sbw}V_x\delta_{driver}}{l_f + l_r} \quad (5)$$

The control architecture of this SbW controller is summarized in Figure 4.

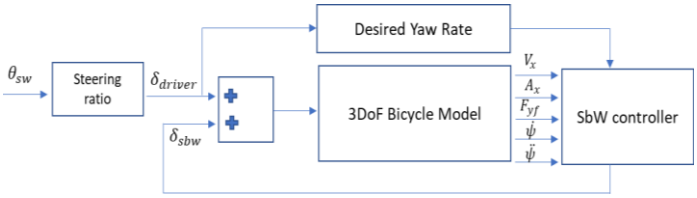

Figure 4: Control scheme for the feedback controller

STEER-BY-WIRE FEEDFORWARD CONTROLLER

The purpose of a reference shaping controller lies within the damping of the self-induced transient disturbances, for instance oscillations in linear or quasi-linear dynamic systems. A vehicle typically exhibits oscillatory behavior due to its inertia during high speed maneuvers such as lane change, double lane change, and Fishhook. This swaying motion might be exacerbated by unnecessary or rather uncoordinated inputs from the driver or planner.

A feedforward pre-filtering technique such as reference shaping is advantageous in terms of computational cost, design complexity and hardware requirements as it is based upon a convolution of the driver inputs with a series of designed impulses. As an open-loop design, it is also capable of operating in the absence or under the influence of corrupted measurements.

In this study, we compose this controller based on the parameters of a nonlinear bicycle model that has been linearized under the assumption of small steering angles and constant longitudinal velocity. The equations shown below are an adaptation from [17] and have been applied specifically to the vehicle stability scenario.

In the design process of a reference shaping control algorithm, the first step is to ensure zero yaw oscillations in the system under maneuvering. This is achieved by adding a secondary impulse to counteract the transient disturbances arising from the first impulse response. Given a system's approximate natural frequency ω_n and damping ratio ζ, the fluctuation caused by a sequence of impulses can be calculated as

$$V(\omega_n, \zeta) = e^{-\zeta\omega_n t_n}\sqrt{C(\omega_n, \zeta)^2 + S(\omega_n, \zeta)^2} \quad (6)$$

where

$$C(\omega_n, \zeta) = \sum_{i=1}^{n} A_i e^{-\zeta\omega_n t_i}\cos(\omega_d t_i) \quad (7)$$

$$S(\omega_n, \zeta) = \sum_{i=1}^{n} A_i e^{-\zeta\omega_n t_i}\sin(\omega_d t_i)\,. \quad (8)$$

Here, A_i and t_i are the amplitudes and execution times of the impulse series whereas n is the total number. As usual, $\omega_d = \omega\sqrt{1-\zeta^2}$ is the damped natural frequency of the system.

By requiring $V(\omega_n, \zeta) = 0$, we can solve for the unknown amplitudes and placement times. Ideally, this sequence will result in zero undesired transients, such as oscillations, in the system when applied. To avoid converge of the above solutions to zero or infinity, certain constraints on the impulse amplitudes, i.e.

$$\sum A_i = 1 \text{ and } A_i > 0 \quad . \quad (9)$$

For this study, we have implemented a two-impulse scheme (n=2) for the SbW controller. Assuming the first input to be applied at $t_1 = 0$ with an amplitude A_1, we must solve for A_1, A_2 and t_2 by fulfilling the condition that (6)-(8) equal 0, i.e.

$$A_1 + A_2 e^{-\zeta\omega_n t_2}\cos(\omega_d t_2) = 0 \quad (10)$$

$$A_2 e^{-\zeta\omega_n t_2}\sin(\omega_d t_2) = 0 \quad . \quad (11)$$

The final solution is then given as

$$\begin{bmatrix} A_i \\ t_i \end{bmatrix} = \begin{bmatrix} \frac{1}{1+K} & \frac{K}{1+K} \\ 0 & 0.5T_d \end{bmatrix} \quad (12)$$

where i=1,2, and T_d is the damped period of vibration with $K = \exp(\frac{-\zeta\pi}{\sqrt{1-\zeta^2}})$. The complete derivation can be found in [13].

This procedure is now applied to a linearized bicycle model, where the system matrix is given by

$$A_{bicycle} = \begin{bmatrix} -\frac{C_{\alpha f} + C_{\alpha r}}{mV} & \frac{l_r C_{\alpha r} - l_f C_{\alpha f}}{mV^2} - 1 \\ \frac{l_r C_{\alpha r} - l_f C_{\alpha f}}{I_{zz}} & -\frac{{l_f}^2 C_{\alpha f} + {l_r}^2 C_{\alpha r}}{I_{zz} V} \end{bmatrix}$$

The natural frequency of the system ω_n, damping ratio ζ, damped natural frequency ω_d, and the time period (T_d) of the damped system are given by

$$\omega_n = \sqrt{A_{11}A_{22} - A_{12}A_{21}} \quad (13)$$

$$\zeta = -\frac{A_{11}+A_{22}}{2\omega_n} \quad (14)$$

$$\omega_d = \omega_n\sqrt{1-\zeta^2} \quad (15)$$

$$T_d = \frac{2\pi}{\omega_d}. \quad (16)$$

Here, V is the tangential velocity of the vehicle with respect to the road curvature, i.e. $\sqrt{V_x^2 + V_y^2}$. Lastly, $C_{\alpha f}$ and $C_{\alpha r}$ are the cornering stiffnesses at the front and rear tires, respectively, which are approximated to be 16.5% of tire load per radian of slip angle as per [14], in turn yielding

$$C_{\alpha f} = 0.165 * 57.29578 * m * g * d_f \quad (17)$$

$$C_{\alpha r} = 0.165 * 57.29578 * m * g * d_r \quad (18)$$

where d_f, d_r are front and rear load distribution ratios for the vehicle ($d_f + d_r = 1$). This provides all parameters necessary to design a two impulse reference shaper. The feedforward controller was tested against the 6 DoF vehicle plant by itself as well as in conjecture with the feedback controller, as presented in Figure 5.

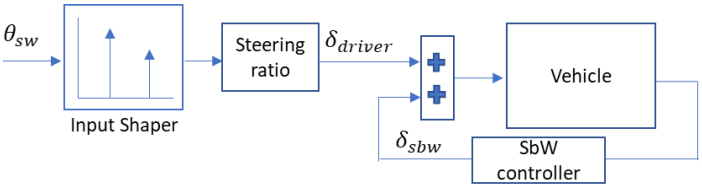

Figure 5: The proposed control scheme for the feedforward controller combined with the feedback law

NUMERICAL RESULTS

The controllers' merits can only be tested in situations challenging to the vehicle's yaw limits. The 'Double Lane Change (DLC)' maneuver is chosen as it is a standard test used to evaluate active safety systems such as ESC. We present and discuss the effect of the controllers designed above in this scenario. Figure 6 depicts the handwheel angle profile selected for the DLC test. We design the maneuver particularly aggressive for the given vehicle speed as to cause dangerous inputs to the system similar to sudden evasive or emergency maneuvers in high speed driving. The chosen speeds are 60 kph and 80 kph.

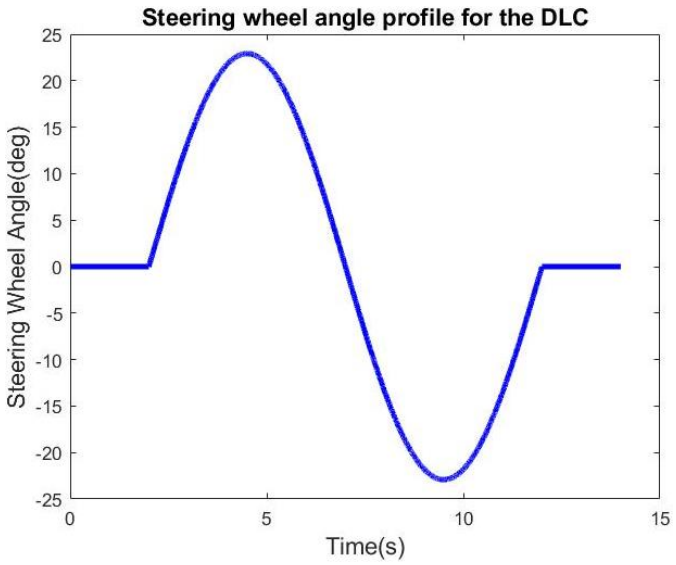

Figure 6: Handwheel angle profile for the DLC test

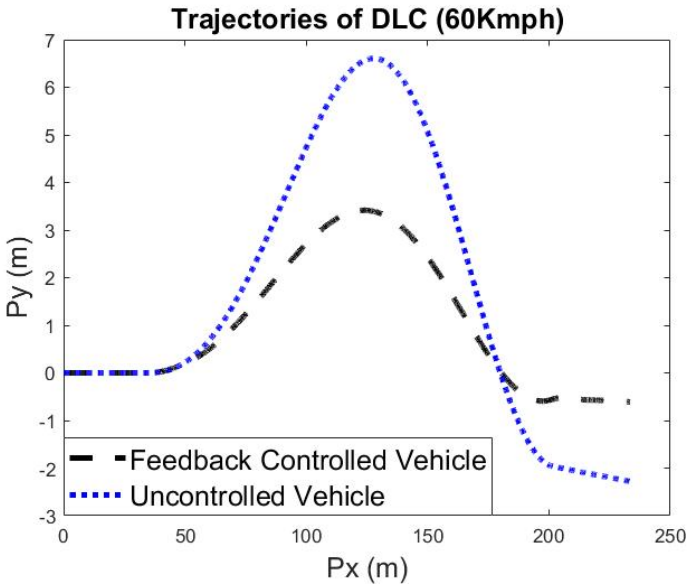

Figure 7: The feedback controller achieving a lateral displacement of less than 3.5m

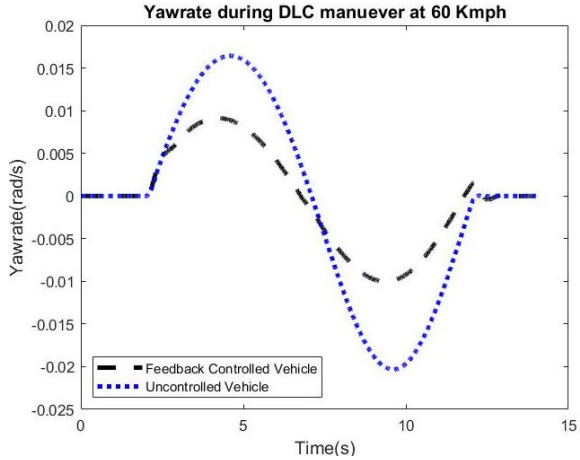

Figure 8: The yaw rate profile during the maneuver at 60 Kmph. Note the spike in the end caused by the controller for stability

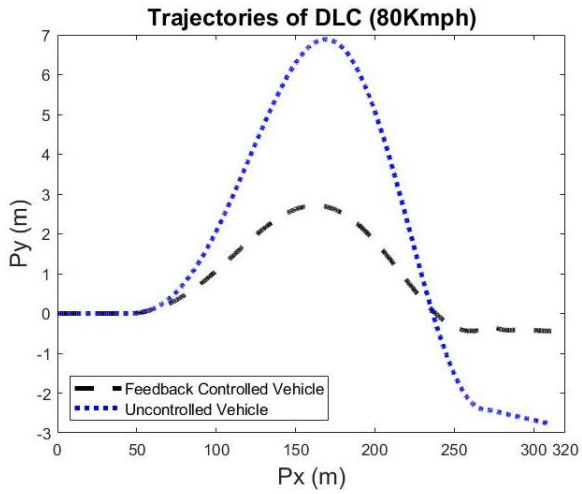

Figure 9: The DLC maneuver at 80 Kmph

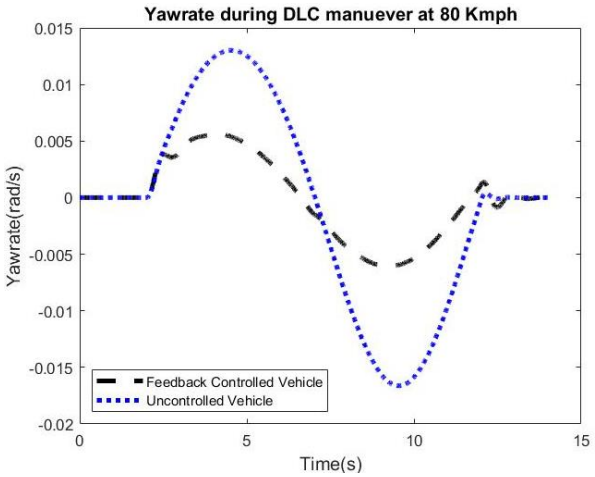

Figure 10: Yaw rate at 80 Kmph DLC

Figures 7-10 illustrate the performance of the feedback controller designed in Section 4. Here, the vehicle can be prevented from skidding while an acceptable yaw rate limit is maintained. The oscillation in yaw rate during the end of the maneuver at 60 and 80 kph (Figures 8 and 10), however, indicate that there are some controller generated transients introduced under abrupt inputs. Furthermore, the feedback controller enforces only the yaw rate to remain under certain limits which could make the maneuver extremely uncomfortable for the passengers. Yet, vehicle behavior can be made smoother utilizing the suggested reference shaping controller as it can filter out bad inputs that cause the system to oscillate and possibly go unstable. The system behavior with the proposed control scheme depicted in Figure 5 are shown in Figures 11-13. Since the feedback controller can handle the maneuver at 80 kph, we will maintain that testing speed henceforth. The feedforward control algorithm convolves a two-impulse sequence with the driver input to cancel out any vibrations in the system. Figures 11-13 also depict the performance of the reference shaper with several other models discussed in this paper.

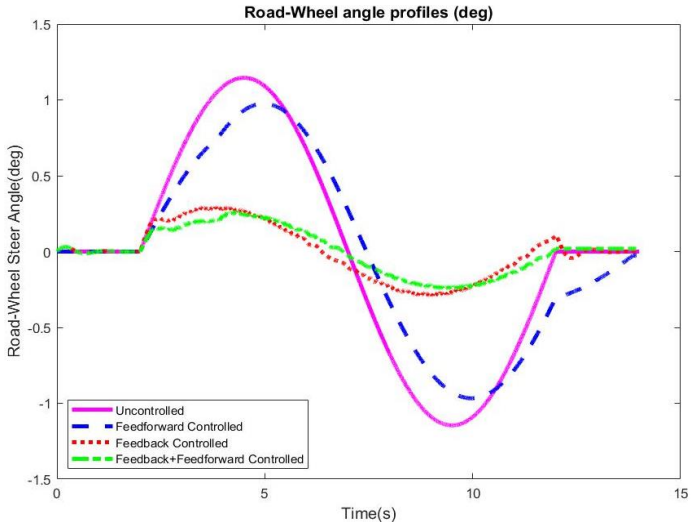

Figure 11: The delta profiles for the different schemes

As depicted in Figure 11, the combination of feedforward control with the available feedback controller yields a significantly reduced total steering input resulting in a reduced total yaw rate. (Figure 13).

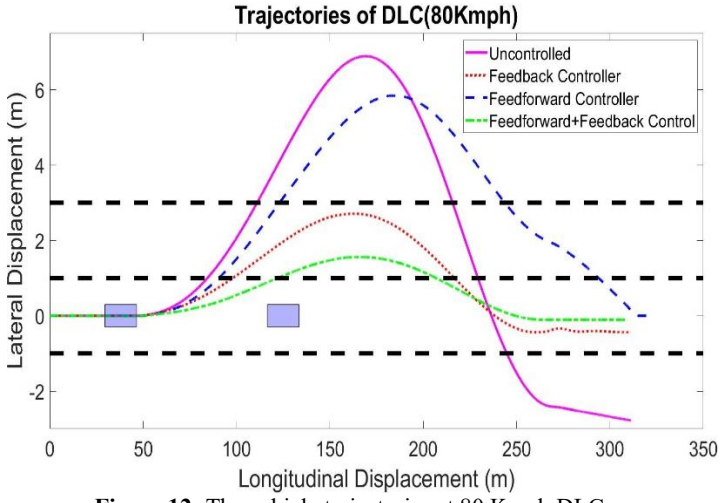

Figure 12: The vehicle trajectories at 80 Kmph DLC

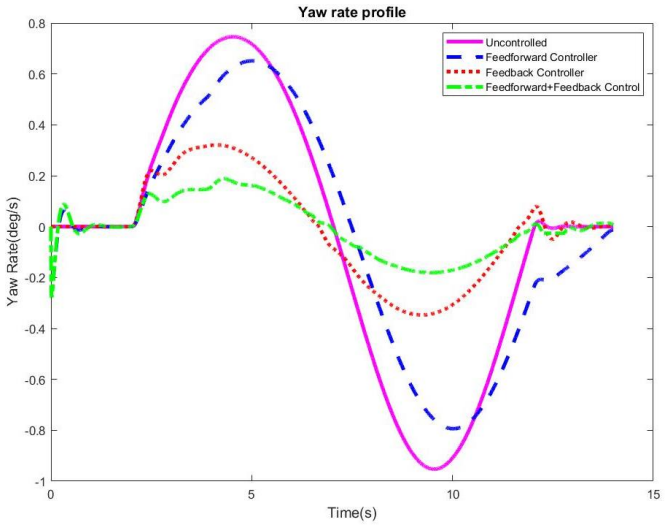

Figure 13: The various yaw rates profiles

DISCUSSION

Observations and Inference

As demonstrated via numerical simulation, the reference shaping feedforward gain combined with the feedback control loop outperforms the feedback controller by itself. This is achieved with insignificant added complexity to the control structure. At the same time, the feedforward control alone also achieves significant performance improvements in comparison to the uncontrolled situations. Note that this is a performance guarantee which can be maintained under total sensor failure. Additionally, it should be noted that the reference shaping control has been designed utilizing a very simple linearized bicycle model while being tested against a 6 DoF non-linear high definition plant that has complex coupled dynamics. The test maneuver is extremely violent (even with respect to severe maneuvers expected in emergency traffic situations) and, as such, highly excites the nonlinear modes and dynamics not captured in the linearized bicycle model. Yet, the reference shaping control manages to capture a significant amount of the inputs causing excessive maneuver reactions and can attenuate the plant's transients. This gives rise to the assumption that a reference shaping control design based upon a higher order model will provide even more robust performance while not adding excessive complexity to the control structure. A brief discussion addressing the key concerns that need to be addressed whilst designing a reference shaper with a highly simplified model and potential methods to address these issues is discussed in the upcoming subsection.

Robust Reference Shaping Control

The method of reference shaping design previously discussed in this study corresponds to a Zero-Vibration (ZV) shaper. Here, the amplitudes and time locations of the impulses depend on the system's natural frequency (ω) and damping ratio (ξ). The ZV shaper's approach explicitly targets specific (undesired) system poles through zero placement and subsequent cancellation. Unfortunately, robustness can be an issue as the design is highly dependent on system parameters, thus modeling errors are highly significant in the presence of such unmodeled errors, the designed impulse sequence tends to cause a non-zero vibration. This lack of robustness with respect to modeling errors could be a major roadblock as the amount of additional vibration increases rapidly if actual frequencies deviate from the modeled frequencies even by small amounts.

However, this can be compensated for by adding a constraint requiring the derivative of the vibration equation (6) to equal zero with respect to the flexible mode frequency, i.e.

$$\frac{d}{d\omega}V(\omega,\zeta) = 0$$

This method is called Zero-Vibration Zero-Derivative (ZVD) and employs placing double zeros at the system poles. This idea can be continued by setting the second derivative of the vibration equation to 0 (differentiated with respect to the frequency).

$$\frac{d^2}{d\omega^2}V(\omega,\zeta) = 0$$

Consequently, the shaper satisfying this additional constraint is called Zero-Vibration Zero-Double Derivative necessitating three zeros at the system poles. The coefficients and time locations of the impulses for each of the three shapers discussed above are presented in Table 1. The resulting controllers based upon the linearized vehicle model are tested on a 6 DoF vehicle model plant illustrated in Figure 14 for comparison.

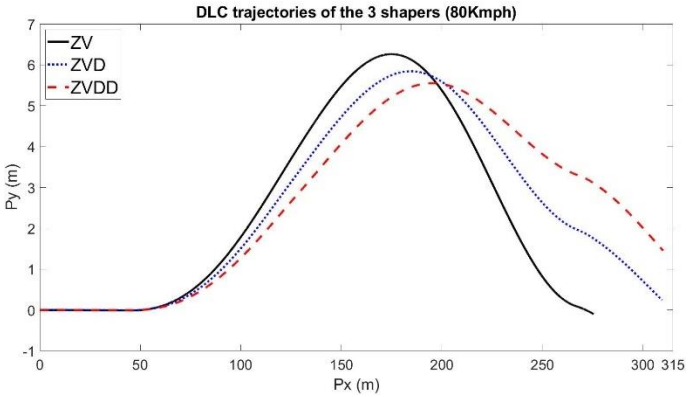

Figure 14: The shapers tested on a 6DoF vehicle dynamics plant

Despite adding several additional constraints for increasing robustness, the non-linearities in the higher order system plant are too significant for the reference shaper based upon a highly simplified linear model. Additionally, the maneuver time increases as more constraints are added to the design. This is not desirable even if the overshoot remains within acceptable limits. Thus, to capture and address the effects of the unstable poles caused by the complex system, further work is necessary.

Table 1: The coefficients and time locations of the impulses for the discussed shaping techniques

Shaper	Coefficients
ZV	$\begin{bmatrix} A_i \\ t_i \end{bmatrix} = \begin{bmatrix} \frac{1}{1+K} & \frac{K}{1+K} \\ 0 & 0.5T_d \end{bmatrix}$
ZVD	$\begin{bmatrix} A_i \\ t_i \end{bmatrix} = \begin{bmatrix} \frac{1}{1+2K+K^2} & \frac{2K}{1+2K+K^2} & \frac{K^2}{1+2K+K^2} \\ 0 & 0.5T_d & T_d \end{bmatrix}$
ZVDD	$[t_i] = [0 \quad 0.5T_d \quad T_d \quad 1.5T_d]$ $A_1 = \frac{1}{1+3K+3K^2+K^3}, A_2 = \frac{3K}{1+3K+3K^2+K^3}$ $A_3 = \frac{3K^2}{1+3K+3K^2+K^3}, A_4 = \frac{K^3}{1+3K+3K^2+K^3}$

Future Work

Even though the controller can be made more robust by adding more insensitivity to parameter uncertainty as demonstrated in advanced approaches such as [18,21-22], modeling errors will always be detrimental for robust control, and pursuing these methods increases the design complexity further. On the other hand, systems with parameter uncertainty and complex non-linear dynamics are prime application areas for adaptive control which has been proven to be effective in coping with modeling errors and parameter uncertainties. Adaptive control schemes can be deployed to determine coefficients for the input shaper and update them on-line.

Another possible technique to increase the robustness of the reference shaper to parameter uncertainties is to build an online parameter estimation framework using a non-linear observer. This observer can be deployed to update the unknown parameters of the linearized system on-the-fly hence increasing the robustness of the shaper. Adaptive control techniques and parameter estimation are the directions we will pursue in future work.

REFERENCES

1. Wissing, C., Nattermann, T., Glander, K. H., & Bertram, T. (2018). Trajectory Prediction for Safety Critical Maneuvers in Automated Highway Driving. *IEEE Conference on Intelligent Transportation Systems, Proceedings, ITSC*, *2018–November*, 131–136. https://doi.org/10.1109/ITSC.2018.8569296
2. Phanomchoeng, G., Zemouche, A., & Rajamani, R. (2017). Real-time automotive slip angle estimation with extended H∞ circle criterion observer for nonlinear output system. *Proceedings of the American Control Conference*, 1636–1641. https://doi.org/10.23919/ACC.2017.7963187
3. Onoda, Y., Onuma, Y., Goto, T., & Sugitani, T. (2010). Design Concept and Advantages of Steer-by-Wire System. *SAE Technical Paper Series*, *1*(724). https://doi.org/10.4271/2008-01-0493
4. infinitis-drive-by-wire-system-gets-upgraded-in-2018-q50-red-sport-400 @ www.foxnews.com. (n.d.). Retrieved from http://www.foxnews.com/auto/2017/11/20/infinitis-drive-by-wire-system-gets-upgraded-in-2018-q50-red-sport-400.html
5. Research-Markets-Global-Automotive-Steering-System-Market @ www.businesswire.com. (n.d.). Retrieved from https://www.businesswire.com/news/home/20150922006166/en/Research-Markets-Global-Automotive-Steering-System-Market
6. Kelling, N. A., & Leteinturier, P. (2019). X-by-Wire : Opportunities , Challenges and Trends, (724).
7. Zhao, W., Qin, X., & Wang, C. (2018). Yaw and Lateral Stability Control for Four-Wheel Steer-by-Wire System. *IEEE/ASME Transactions on Mechatronics*, *23*(6), 2628–2637. https://doi.org/10.1109/TMECH.2018.2812220
8. Han, S., & Baek, J. (2015). A receding horizon yaw moment control law for steer-by-wire and independent drive vehicles. *2015 IEEE Conference on Control and Applications, CCA 2015 - Proceedings*, 1697–1701. https://doi.org/10.1109/CCA.2015.7320854
9. Wang, H., He, P., Yu, M., Liu, L., Do, M. T., Kong, H., & Man, Z. (2016). Adaptive neural network sliding mode control for steer-by-wire-based vehicle stability control. *Journal of Intelligent and Fuzzy Systems*, *31*(2), 885–902. https://doi.org/10.3233/JIFS-169019
10. Daher, N., & Ivantysynova, M. (2015). Yaw stability control of articulated frame off-highway vehicles via displacement controlled steer-by-wire. *Control Engineering Practice*, *45*, 46–53. https://doi.org/10.1016/j.conengprac.2015.08.011
11. Gürleyük, S. S., Bahadir, Ö., Türkkan, Y., & Üşenti, H. (2008). Improved three-step input shaping control of crane system. *WSEAS Transactions on Systems*, *7*(6), 652–661.
12. Singhose, W., Kim, D., & Kenison, M. (2008). Input Shaping Control of Double-Pendulum Bridge Crane Oscillations. *Journal of Dynamic Systems, Measurement, and Control*, *130*(3), 034504. https://doi.org/10.1115/1.2907363
13. MATLAB Release 2018b, The MathWorks, Inc., Natick, Massachusetts, United States.
14. Bakker, E., Pacejka, H. B., & Lidner, L. (1989). Vehicle Dynamics Studies. *SAE International*, 890087.
15. NHTSA. (2013). Laboratory Test Procedure for Dynamic Rollover The Fishhook Maneuver Test Procedure. *U.S. Department of Transportation*, (March), 1–43.
16. Rajamani, Rajesh. *Vehicle Dynamics and Control*. Springer, 2012.
17. Singh, T., & Singhose, W. (2002). Input shaping/time delay control of maneuvering flexible structures. *Proceedings of the 2002 American Control Conference (IEEE Cat. No.CH37301)*, 1717–1731 vol.3. https://doi.org/10.1109/ACC.2002.1023813
18. Berntorp K. Derivation of a six degrees-of-freedom ground-vehicle model for automotive applications. Technical Report ISRN LUTFD2/TFRT–7627–SE, Department of Automatic Control, Sweden: Lund University; 2013.
19. Schindler E. Fahrdynamik: Grundlagen Des Lenkverhaltens Und Ihre Anwendung Für Fahrzeugregelsysteme. Renningen: Expert-Verlag; 2007.
20. N. Singer and W. Seering. Vibration reduction using multi-hump extra insensitive input shapers. In *Proceedings of the*

1995 American Control Conference, Seattle, WA, volume 5, pages 3830–3834, 1995.
21. Liu, S-W., and Singh, T., 1997, "Robust Time-Optimal Control of Nonlinear Structures with Parameter Uncertainties", ASME J. of Dynamic Systems, Measurement and Control, Vol. 119, No. 4, 1997, pp 743-748.
22. Solatges, T., Rubrecht, S., Rognant, M., & Bidaud, P. (2017). Adaptive input shaper design for flexible robot manipulators. 2017 IEEE/RSJ International Conference on Intelligent Robots and Systems (IROS). doi:10.1109/iros.2017.8202191

APPENDIX

VEHICLE DYNAMICS MODELS

Nomenclature

l_f	Distance from front axle to CG	*m*
l_r	Distance from rear axle to CG	*m*
w	½ of the wheelbase of vehicle	*m*
m	Mass of vehicle	*kg*
I_{xx}	Vehicle chassis inertia X	*kg m²*
I_{yy}	Vehicle chassis inertia Y	*kg m²*
I_{zz}	Vehicle chassis inertial Z	*kg m²*
R_w	Wheel radius	*m*
I_w	Wheel inertia	*kg m²*
σ	Tire relaxation length	*m*
g	Acceleration due to gravity	ms^{-2}
h	Distance between roll center and mass center	*m*
$K_{\phi f}, K_{\phi r}$	Roll moment parameters	$Nm(rad)^{-1}$
$D_{\phi f}, D_{\phi r}$	Roll moment parameters	$Nms(rad)^{-1}$
K_θ	Pitch moment parameter	$Nm(rad)^{-1}$
D_θ	Pitch moment parameter	$Nms(rad)^{-1}$
$\alpha_{f,r}$	Slip angles front and rear	*rad*
$\omega_{f,r}$	Wheel speeds front and rear	*rad/s*
θ	Theta is the pitch	*rad*
φ	Phi is the roll	*rad*
ψ	Psi is the yaw	*rad*
V_x	Longitudinal velocity	*m/s*
V_y	Lateral velocity	*m/s*
$V_{x,fr}$	Longitudinal velocity at front and rear axle	*m/s*
$V_{y,fr}$	Lateral velocity at front and rear axle	*m/s*
F_z / $F_{z,fr}$	Normal forces at CG, front and rear	$Kg\ ms^{-2}$
F_x / $F_{x,fr}$	Longitudinal force at CG, front and rear tires	$Kg\ ms^{-2}$
F_y / $F_{y,fr}$	Lateral forces at CG, front and rear tires	$Kg\ ms^{-2}$
$T_{f,r}$	Front and rear driving/braking torques	*Nm*
δ	Road wheel steer angle	*rad*
θ_{SW}	Hand wheel steer angle	*rad*
$C_{\alpha,fr}$	Cornering stiffness front and rear	*Kg/rad*

Non-linear bicycle model

The non-linear bicycle model consists of 2 translational and 1 rotational degrees of freedom. The derivation and free body diagram (FBD) are detailed in [19].

Equations of motion for the chassis:

$$\dot{V}_x = \frac{F_X}{m} + V_y\dot{\psi}$$

$$\dot{V}_y = \frac{F_Y}{m} - V_x\dot{\psi}$$

$$\ddot{\psi} = \frac{M_Z}{I_{zz}}$$

$F_X = F_{xf} + F_{xr}$, $\mathrm{F_Y} = \mathrm{F_{yf}} + \mathrm{F_{yr}}$ and $\mathrm{M_Z} = \mathrm{l_f}(\mathrm{F_{yf}})\text{-}\mathrm{l_r}(\mathrm{F_{yr}})$
The normal forces at front and rear are given by $F_{zf} = \frac{mgl_r}{l}$ and $F_{zr} = \frac{mgl_f}{l}$, where $\mathrm{l} = \mathrm{l_f} + \mathrm{l_r}$.

Equations of motion for the wheels and tires:

The slip-angles, slip ratios and wheel speeds are given by

$$\dot{\alpha}_{f,r} = \left(-\arctan\left(\frac{V_{yf,r}}{V_{xf,r}}\right) - \alpha_{f,r}\right)\frac{V_{xf,r}}{\sigma}$$

$$\kappa_{f,r} = \frac{R_w\omega_{f,r} - V_{xf,r}}{V_{xf,r}}$$

$$\dot{\omega}_{f,r} = \frac{T_{f,r} - R_w F_{xf,r}}{I_w}$$

where $\begin{bmatrix} V_{yf} \\ V_{xf} \end{bmatrix} = \begin{bmatrix} cos\delta & -sin\delta \\ sin\delta & cos\delta \end{bmatrix}\begin{bmatrix} V_y + l_f\dot{\psi} \\ V_x \end{bmatrix}$

and $\begin{bmatrix} V_{yr} \\ V_{xr} \end{bmatrix} = \begin{bmatrix} cos\delta & -sin\delta \\ sin\delta & cos\delta \end{bmatrix}\begin{bmatrix} V_y - l_r\dot{\psi} \\ V_x \end{bmatrix}$.

The nominal tire forces according to the Magic formula [15] yield

$$F_{x0f,r} = \mu_{xf,r}F_{zf,r}\sin\Big(C_{xf,r}\,arctan\Big(B_{xf,r}\kappa_{f,r} - E_{xf,r}\big(B_{xf,r}\kappa_{f,r} - arctan\big(B_{xf,r}\kappa_{f,r}\big)\big)\Big)\Big)$$

$$F_{y0f,r} = \mu_{yf,r} F_{zf,r} \sin\Big(C_{yf,r}\, arctan\Big(B_{yf,r}\alpha_{f,r} - E_{yf,r}\big(B_{yf,r}\alpha_{f,r} - arctan\big(B_{yf,r}\alpha_{f,r}\big)\big)\Big)\Big) .$$

The lateral combined forces are given by the friction ellipse, i.e.

$$F_{yf,r} = F_{y0f,r}\sqrt{1 - \left(\frac{F_{x0f,r}}{\mu_{xf,r}F_{zf,r}}\right)^2} .$$

The longitudinal combined forces and the rotated lateral combined forces are given by

$F_{xf} = F_{x0f}cos\delta - F_{yf}sin\delta$ and $F_{xr} = F_{x0r}$

$F_{yf} = F_{yf}cos\delta + F_{x0f}sin\delta$ and $F_{yr} = F_{yr}$

Four-wheel vehicle model

For the derivation of the four-wheel vehicle model equations of motion, the reader is referred to [20].

Equations of Motion for the Chassis:

$$\dot{V}_x = h\big[\big(\dot{\psi} + \dot{\phi} + \dot{\theta}\big)sin\theta cos\phi - \ddot{\psi}sin\phi - 2\dot{\phi}\dot{\psi}cos\phi - \ddot{\theta}cos\theta cos\phi + 2\dot{\theta}\dot{\phi}cos\theta sin\phi + \ddot{\phi}sin\theta sin\phi\big] + \frac{F_X}{m} + V_y\dot{\psi}$$

$$\dot{V}_y = h\big[-\ddot{\psi}sin\theta cos\phi - \dot{\psi}^2 sin\phi - 2\dot{\psi}\dot{\theta}cos\theta cos\phi + \dot{\psi}\dot{\phi}sin\theta sin\phi - \dot{\phi}^2 sin\phi + \ddot{\phi}cos\phi\big] + \frac{F_Y}{m} - V_x\dot{\psi}$$

$$\ddot{\psi} = \frac{(M_Z - h(F_X sin\phi + F_Y sin\theta cos\phi))}{(I_{xx}sin^2\theta + cos^2\theta(I_{yy}sin^2\phi + I_{zz}cos^2\phi))}$$

$$\ddot{\theta} = (-K_\theta\theta - D_\theta\dot{\theta} + h[mgsin\theta cos\phi - F_X cos\theta cos\phi] + \dot{\psi}\big[\dot{\psi}sin\theta cos\theta\big(\Delta I_{xy} + cos^2\phi\Delta I_{yz}\big) - \dot{\phi}\big(I_{xx}cos^2\theta + I_{yy}sin^2\theta sin^2\phi + I_{zz}sin^2\theta cos^2\phi\big) - \dot{\theta}\big(\Delta I_{yz}sin\theta sin\phi cos\phi\big)\big])/(I_{yy}cos^2\phi + I_{zz}sin^2\phi)$$

$$\ddot{\phi} = (-K_\phi\phi - D_\phi\dot{\phi} + h[F_Y cos\phi cos\theta + mgsin\phi] + \Delta I_{yz}\dot{\psi}\big[\dot{\psi}sin\phi cos\phi cos\theta + \dot{\phi}sin\theta sin\phi cos\phi\big] + \dot{\psi}\dot{\theta}I_{yy}cos^2\phi + I_{zz}sin^2\phi)/(I_{xx}cos^2\theta + I_{yy}sin^2\theta sin^2\phi + I_{zz}sin^2\theta cos^2\phi)$$

$F_X = F_{x1} + F_{x2} + F_{x3} + F_{x4}$, $F_Y = F_{y1} + F_{y2} + F_{y3} + F_{y4}$ and $M_Z = l_f\big(F_{y1} + F_{y2}\big) - l_r\big(F_{y3} + F_{y4}\big) + w(F_{x2} - F_{x1}) - w(F_{x3} + F_{x4})$

The normal forces at the wheels are given by solving the set of following 4 equations:

$$(F_{z1} + F_{z2})l_f - (F_{z3} + F_{z4})l_r = K_\theta\theta + D_\theta\dot{\theta}$$

$$F_{z1} + F_{z2} + F_{z3} + F_{z4} = mg$$

$$F_{z2} - F_{z1} = \frac{K_{\phi f}\phi + D_{\phi f}\dot{\phi}}{w}$$

$$F_{z4} - F_{z3} = \frac{K_{\phi r}\phi + D_{\phi r}\dot{\phi}}{w}$$

Equations of motion for the individual wheels and tires:

The slip angles, slip ratios and wheel speeds yield (i=1,2,3,4)

$$\dot{\alpha}_i = \left(-\arctan\left(\frac{V_{yi}}{V_{xi}}\right) - \alpha_i\right)\frac{V_{xi}}{\sigma}$$

$$\kappa_i = \frac{R_w\omega_i - V_{xi}}{V_{xi}}$$

$$\dot{\omega}_i = \frac{T_i - R_w F_{xi}}{I_w}$$

Where $\begin{bmatrix}V_{y1}\\V_{x1}\end{bmatrix} = \begin{bmatrix}cos\delta & -sin\delta\\ sin\delta & cos\delta\end{bmatrix}\begin{bmatrix}V_y + l_f\dot{\psi}\\V_x - w\dot{\psi}\end{bmatrix}$,

$\begin{bmatrix}V_{y2}\\V_{x2}\end{bmatrix} = \begin{bmatrix}cos\delta & -sin\delta\\ sin\delta & cos\delta\end{bmatrix}\begin{bmatrix}V_y + l_f\dot{\psi}\\V_x + w\dot{\psi}\end{bmatrix}$,

$\begin{bmatrix}V_{y3}\\V_{x3}\end{bmatrix} = \begin{bmatrix}cos\delta & -sin\delta\\ sin\delta & cos\delta\end{bmatrix}\begin{bmatrix}V_y - l_r\dot{\psi}\\V_x - w\dot{\psi}\end{bmatrix}$,

and $\begin{bmatrix}V_{y4}\\V_{x4}\end{bmatrix} = \begin{bmatrix}cos\delta & -sin\delta\\ sin\delta & cos\delta\end{bmatrix}\begin{bmatrix}V_y - l_r\dot{\psi}\\V_x + w\dot{\psi}\end{bmatrix}$.

The nominal tire forces according to the Magic formula result in

$$F_{x0i} = \mu_{xi}F_{zi}\sin\big(C_{xi}\, arctan\big(B_{xi}\kappa_i - E_{xi}(B_{xi}\kappa_i - arctan(B_{xi}\kappa_i))\big)\big)$$

$$F_{y0i} = \mu_{yi}F_{zi}\sin\Big(C_{yi}\, arctan\Big(B_{yi}\alpha_i - E_{yi}\big(B_{yi}\alpha_i - arctan\big(B_{yi}\alpha_i\big)\big)\Big)\Big) .$$

The lateral combined forces are given by the friction ellipse, i.e.

$$F_{yi} = F_{y0i}\sqrt{1 - \left(\frac{F_{x0i}}{\mu_{xi}F_{zi}}\right)^2} .$$

The rotated combined forces are given by

$$\begin{bmatrix}F_{x1,2}\\F_{y1,2}\end{bmatrix} = \begin{bmatrix}cos\delta & -sin\delta\\ sin\delta & cos\delta\end{bmatrix}\begin{bmatrix}F_{x01,2}\\F_{y1,2}\end{bmatrix} \text{ and } \begin{bmatrix}F_{x3,4}\\F_{y3,4}\end{bmatrix} = \begin{bmatrix}F_{x03,4}\\F_{y3,4}\end{bmatrix}.$$